Inverse Problems **16** (2000) 1297–1322. Printed in the UK PII: S0266-5611(00)14585-X

# 3D electromagnetic inversion based on quasi-analytical approximation

Michael Zhdanov† and Gabor Hursan
University of Utah, Department of Geology and Geophysics, Salt Lake City, UT 84112, USA

Received 3 March 2000

**Abstract.** In this paper we address one of the most challenging problems of electromagnetic (EM) geophysical methods: three-dimensional (3D) inversion of EM data over inhomogeneous geological formations. The difficulties in the solution of this problem are two-fold. On the one hand, 3D EM forward modelling is an extremely complicated and time-consuming mathematical problem itself. On the other hand, the inversion is an unstable and ambiguous problem. To overcome these difficulties we suggest using, for forward modelling, the new quasi-analytical (QA) approximation developed recently by Zhdanov *et al* (Zhdanov M S, Dmitriev V I, Fang S and Hursan G 1999 *Geophysics* at press). It is based on ideas similar to those developed by Habashy *et al* (Habashy T M, Groom R W and Spies B R 1993 *J. Geophys. Res.* **98** 1759–75) for a localized nonlinear approximation, and by Zhdanov and Fang (Zhdanov M S and Fang S 1996a *Geophysics* **61** 646–65) for a quasi-linear approximation. We assume that the anomalous electrical field within an inhomogeneous domain is linearly proportional to the background (normal) field through a scalar electrical reflectivity coefficient, which is a function of the background geoelectrical cross-section and the background EM field only. This approach leads to construction of the QA expressions for an anomalous EM field and for the Frechet derivative operator of a forward problem, which simplifies dramatically the forward modelling and inversion. To obtain a stable solution of a 3D inverse problem we apply the regularization method based on using a focusing stabilizing functional introduced by Portniaguine and Zhdanov (Portniaguine O and Zhdanov M S 1999 *Geophysics* **64** 874–87). This stabilizer helps generate a sharp and focused image of anomalous conductivity distribution. The inversion is based on the re-weighted regularized conjugate gradient method.

## 1. Introduction

Electromagnetic (EM) geophysical methods are widely used in the study of the internal structure of the earth in mineral, oil and gas prospecting, tectonic studies, and environmental assessment and monitoring. They provide unique information about the geological structures, petrophysical properties, lithologic characteristics, and thermodynamic and phase status of the rocks in the Earth's interior. The future perspective in EM geophysical methods lies in the development of multi-transmitter and multi-receiver methods with an array observation system analogous to a seismic data acquisition system. Therefore, the main efforts in the development of an interpretation technique has to be concentrated on creating three-dimensional (3D) methods of analysis of the array EM data. At the same time, the development of effective interpretation schemes for 3D inhomogeneous geological structures is still one of the most challenging problems in geophysics.

During the last decade, considerable advances have been made in forward modelling, especially in 3D cases (Madden and Mackie 1989, Wannamaker 1991, Xiong 1992, Newman

† To whom correspondence should be addressed.

0266-5611/00/051297+26$30.00  

and Alumbaugh 1997, Avdeev *et al* 1998, Druskin *et al* 1999). Also, we can observe remarkable progress in the development of a multi-dimensional interpretation technique. Several papers have been published during the last few years on 3D inversion of EM data (Eaton 1989, Madden and Mackie 1989, Smith and Booker 1991, Lee and Xie 1993, Oristaglio *et al* 1993, Pellerin *et al* 1993, Nekut 1994, Torres-Verdin and Habashy 1994, Zhdanov and Keller 1994, Xie and Lee 1995, Newman and Alumbaugh 1997, Zhdanov and Fang 1996b, 1999 and Alumbaugh and Newman 1997). Note that this reference list includes the papers which focus on inversion in the Earth and are most relevant to our paper only.

The methods for solving multi-dimensional EM inverse problems are usually based on the optimization of the model parameters by applying different inversion schemes. The key problems in the optimization technique is the calculation of the Frechet derivative (sensitivity matrix), which usually requires a lot of computational time.

Thus, speaking about the future perspective on developments in EM research, we should emphasize that the main goal will be multi-dimensional modelling and inversion, oriented to the use of the array EM data. In this connection one of the key problems is the speed of multi-dimensional modelling codes. A powerful tool for EM numerical modelling and inversion is the integral equation method (Hohmann 1975, Weidelt 1975, Dmitriev and Pozdnyakova 1992). This method is based on the reduction of the EM problem to a system of integral equations with respect to the excess current $j^e$ within the inhomogeneity. The main difficulty of this technique is related to the large size of the matrix of the linear system of equations, which could require a great deal of computer memory and time for calculations.

Another way to overcome this problem is to use the Born-type approximations for fast forward modelling (Born 1933, Habashy *et al* 1993, Torres-Verdin and Habashy 1994). These approximate, but accurate enough, forward solutions provide a linear forward modelling operator which can be used for the rapid inversion of the multi-dimensional data (Berdichevsky and Zhdanov 1984, Habashy *et al* 1986, Oristaglio 1989). Habashy *et al* (1993) developed a generalized Born approximation (so-called localized nonlinear (LN) approximation), which improved significantly the accuracy of the approximate solutions, and applied it to inversion (Torres-Verdin and Habashy 1994). In our recent publications, (Zhdanov and Fang 1996a, b, 1997, 1999), we modified this approach to 3D EM modelling and inversion, introducing a quasi-linear (QL) approximation. Within the framework of this method, the anomalous electrical field inside an inhomogeneous domain is linearly proportional to the background (normal) field through an electrical reflectivity tensor $\hat{\lambda}$, which is a function of the background geoelectrical cross-section and the background EM field only. The electrical reflectivity tensor $\hat{\lambda}$ can be determined by an approximate analytical solution of the corresponding integral equation (Zhdanov *et al* 1999). This approach leads to a construction of the quasi-analytical (QA) expressions for an anomalous EM field and the Frechet derivative operator of a forward problem, which simplifies dramatically the forward EM modelling and inversion for inhomogeneous geoelectrical structures.

Another critical problem in inversion of EM data is developing a stable inverse problem solution which can produce, at the same time, a sharp and focused image of the target. The traditional inversion methods are usually based on the Tikhonov regularization theory, which provides a stable solution of the inverse problem. This goal is reached, as a rule, by introducing a maximum smoothness stabilizing functional. The obtained solution provides a smooth image, which in many practical situations does not describe the examined object properly.

Recently, a new approach to reconstruction of noisy images has been developed in a number of papers (Rudin *et al* 1992, Vogel and Oman 1998). It is based on a total variational stabilizing functional which requires that the model parameter distribution be of bounded variation. This requirement is much weaker than one of maximum smoothness because it can be applied even to discontinuous functions. In this way the total variation method produces better quality images for blocky structures. However, it still decreases the boundaries of the model parameter variation and therefore distorts the real image.

We consider different ways of focusing EM images using specially selected stabilizing functionals. In particular, we use a new stabilizing functional which minimizes the area where strong model parameter variations and discontinuity occur. This functional was originally introduced for the solution of a gravity inverse problem (Portniaguine and Zhdanov 1999). We call this new functional a focusing stabilizer. We demonstrate how the focusing stabilizer helps to generate a stable solution of the EM inverse problem for complex objects and helps to generate much more 'focused' EM images than conventional methods.

Thus, the main goal of this paper is to demonstrate that a relatively simple QA expression for EM response over arbitrary 3D inhomogeneous structures, derived by Zhdanov *et al* (1999), in combination with the focusing stabilizer, can be used for developing a new generation of fast 3D EM inversion techniques.

## 2. QA solutions for a 3D EM field

For completeness, we begin our paper with the formulation of the basic principles of QL and QA approximations. Consider a 3D geoelectrical model with a background (normal) complex conductivity $\tilde{\sigma}_b$ and local inhomogeneity $D$ with the arbitrary spatial variations of complex conductivity $\tilde{\sigma} = \tilde{\sigma}_b + \Delta\tilde{\sigma}$. We assume that $\mu = \mu_0 = 4\pi \times 10^{-7}$ H m$^{-1}$, where $\mu_0$ is the free-space magnetic permeability. The model is excited by an EM field generated by an arbitrary source. This field is time harmonic as $e^{-i\omega t}$. Complex conductivity includes the effect of displacement currents: $\tilde{\sigma} = \sigma - i\omega\varepsilon$, where $\sigma$ and $\varepsilon$ are electrical conductivity and dielectric permittivity, respectively. The EM fields in this model can be presented as a sum of background (normal) and anomalous fields:

$$\boldsymbol{E} = \boldsymbol{E}^b + \boldsymbol{E}^a, \qquad \boldsymbol{H} = \boldsymbol{H}^b + \boldsymbol{H}^a, \tag{1}$$

where the background field is a field generated by the given sources in the model with the background distribution of conductivity $\tilde{\sigma}_b$, and the anomalous field is produced by the anomalous conductivity distribution $\Delta\tilde{\sigma}$.

It is well known that the anomalous field can be presented as an integral over the excess currents in inhomogeneous domain $D$ (Hohmann 1975, Weidelt 1975):

$$\boldsymbol{E}^a(\boldsymbol{r}_j) = \int_D \hat{\boldsymbol{G}}_E(\boldsymbol{r}_j \mid \boldsymbol{r})\boldsymbol{j}^a(\boldsymbol{r})\,\mathrm{d}v = \boldsymbol{G}_E(\boldsymbol{j}^a), \tag{2}$$

$$\boldsymbol{H}^a(\boldsymbol{r}_j) = \int_D \hat{\boldsymbol{G}}_H(\boldsymbol{r}_j \mid \boldsymbol{r})\boldsymbol{j}^a(\boldsymbol{r})\,\mathrm{d}v = \boldsymbol{G}_H(\boldsymbol{j}^a), \tag{3}$$

where $\hat{\boldsymbol{G}}_E(\boldsymbol{r}_j \mid \boldsymbol{r})$ and $\hat{\boldsymbol{G}}_H(\boldsymbol{r}_j \mid \boldsymbol{r})$ are the electric and magnetic Green tensors defined for an unbounded conductive medium with the background conductivity $\tilde{\sigma}_b$; $\boldsymbol{G}_E$ and $\boldsymbol{G}_H$ are corresponding Green linear operators, and the excess current $\boldsymbol{j}^a$ is determined by the equation

$$\boldsymbol{j}^a = \Delta\tilde{\sigma}\boldsymbol{E} = \Delta\tilde{\sigma}(\boldsymbol{E}^b + \boldsymbol{E}^a). \tag{4}$$

Using Green operators, one can calculate the EM field at any point $\boldsymbol{r}_j$, if the electric field is known within the inhomogeneity.

$$\boldsymbol{E}(\boldsymbol{r}_j) = \boldsymbol{G}_E(\Delta\tilde{\sigma}\boldsymbol{E}) + \boldsymbol{E}^b(\boldsymbol{r}_j), \tag{5}$$

$$\boldsymbol{H}(\boldsymbol{r}_j) = \boldsymbol{G}_H(\Delta\tilde{\sigma}\boldsymbol{E}) + \boldsymbol{H}^b(\boldsymbol{r}_j). \tag{6}$$

Expression (5) becomes the integral equation with respect to electric field $\boldsymbol{E}(\boldsymbol{r})$, if $\boldsymbol{r}_j \in D$.

The QL approximation is based on the assumption that the anomalous field $\boldsymbol{E}^a$ inside the inhomogeneous domain is linearly proportional to the background field $\boldsymbol{E}^b$ through some tensor $\hat{\lambda}$ (Zhdanov and Fang 1996a):

$$\boldsymbol{E}^a(\boldsymbol{r}) \approx \hat{\lambda}(\boldsymbol{r})\boldsymbol{E}^b(\boldsymbol{r}). \tag{7}$$

Note that, in the framework of the QL approach, the electrical reflectivity tensor can be selected to be a scalar one (Zhdanov and Fang 1996a):

$$\hat{\lambda} = \lambda\hat{\boldsymbol{I}}, \tag{8}$$

where $\hat{\boldsymbol{I}}$ is a unit tensor. This assumption, of course, reduces the areas of practical applications of the QA approximations because, in this case, the anomalous (scattered) field is polarized in a direction parallel to the background field within the inhomogeneity. However, in a general case the anomalous field can be polarized in a different direction from the background field, which could generate additional errors in the scalar QA approximation. Therefore, this particular choice may be a cause of difficulties in the case of elongated bodies (e.g. needle-like) or of flat bodies (e.g. plate-like), while strong conductivity contrast could also be a source of errors, as well as fast variations of the background field in the body volume. Nevertheless, numerical modelling demonstrates that the corresponding errors are within a few percentages if observations are conducted in the far zone of the transmitter, or in the case of plane-wave excitation (Zhdanov *et al* 1999).

Substituting formulae (7) and (8) into (5), we obtain the QL approximation $\boldsymbol{E}^a_{\mathrm{QL}}(\boldsymbol{r})$ for the anomalous field:

$$\boldsymbol{E}^a_{\mathrm{QL}}(\boldsymbol{r}_j) = \boldsymbol{G}_E(\Delta\tilde{\sigma}(1+\lambda(\boldsymbol{r}))\boldsymbol{E}^b). \tag{9}$$

The last formula can be used to derive a QL equation with respect to the electrical reflectivity coefficient $\lambda$:

$$\lambda(\boldsymbol{r}_j)\boldsymbol{E}^b(\boldsymbol{r}_j) = \boldsymbol{G}_E[\Delta\tilde{\sigma}\lambda(\boldsymbol{r})\boldsymbol{E}^b] + \boldsymbol{E}^B(\boldsymbol{r}_j), \tag{10}$$

where $\boldsymbol{E}^B(\boldsymbol{r}_j)$ is the Born approximation

$$\boldsymbol{E}^B(\boldsymbol{r}_j) = \boldsymbol{G}_E(\Delta\tilde{\sigma}\boldsymbol{E}^b) = \int_D \hat{\boldsymbol{G}}_E(\boldsymbol{r}_j \mid \boldsymbol{r})\Delta\tilde{\sigma}(\boldsymbol{r})\boldsymbol{E}^b(\boldsymbol{r})\,\mathrm{d}v, \tag{11}$$

and $\boldsymbol{G}_E[\Delta\tilde{\sigma}\lambda(\boldsymbol{r})\boldsymbol{E}^b]$ linearly depends on $\lambda(\boldsymbol{r})$:

$$\boldsymbol{G}_E[\Delta\tilde{\sigma}\lambda(\boldsymbol{r})\boldsymbol{E}^b] = \int_D \hat{\boldsymbol{G}}_E(\boldsymbol{r}_j \mid \boldsymbol{r})\Delta\sigma(\boldsymbol{r})\lambda(\boldsymbol{r})\boldsymbol{E}^b(\boldsymbol{r})\,\mathrm{d}v. \tag{12}$$

Following Habashy *et al* (1993) and Torres-Verdin and Habashy (1994), we can take into account that the Green tensor $\hat{\boldsymbol{G}}_E(\boldsymbol{r}_j \mid \boldsymbol{r})$ exhibits either singularity or a peak at the point where $\boldsymbol{r}_j = \boldsymbol{r}$. Therefore, one can expect that the dominant contribution to the integral $\boldsymbol{G}_E[\Delta\tilde{\sigma}\lambda\boldsymbol{E}^b]$ in equation (10) is from some vicinity of the point $\boldsymbol{r}_j = \boldsymbol{r}$. Assuming also that $\lambda(\boldsymbol{r}_j)$ is a slowly varying function within domain $D$, one can write

$$\lambda(\boldsymbol{r}_j)\boldsymbol{E}^b(\boldsymbol{r}_j) \approx \lambda(\boldsymbol{r}_j)\boldsymbol{G}_E[\Delta\tilde{\sigma}\boldsymbol{E}^b] + \boldsymbol{E}^B(\boldsymbol{r}_j) = \lambda(\boldsymbol{r}_j)\boldsymbol{E}^B(\boldsymbol{r}_j) + \boldsymbol{E}^B(\boldsymbol{r}_j). \tag{13}$$

Taking into account that we are looking for a scalar reflectivity tensor, it is useful to introduce a scalar equation on the basis of the vector equation (13). We can obtain a scalar equation by calculating the dot product of both sides of equation (13) and the background electric field:

$$\lambda(\boldsymbol{r}_j)\boldsymbol{E}^b(\boldsymbol{r}_j)\cdot\boldsymbol{E}^{b*}(\boldsymbol{r}_j) = \lambda(\boldsymbol{r}_j)\boldsymbol{E}^B(\boldsymbol{r}_j)\cdot\boldsymbol{E}^{b*}(\boldsymbol{r}_j) + \boldsymbol{E}^B(\boldsymbol{r}_j)\cdot\boldsymbol{E}^{b*}(\boldsymbol{r}_j), \tag{14}$$

where '*' means complex conjugate vector.

Dividing equation (14) by the square of the background field and assuming that

$$\boldsymbol{E}^b(\boldsymbol{r}_j)\cdot\boldsymbol{E}^{b*}(\boldsymbol{r}_j)\neq 0, \tag{15}$$

we obtain

$$\lambda(\boldsymbol{r}_j)=\frac{g(\boldsymbol{r}_j)}{1-g(\boldsymbol{r}_j)}, \tag{16}$$

where

$$g(\boldsymbol{r}_j)=\frac{\boldsymbol{E}^B(\boldsymbol{r}_j)\cdot\boldsymbol{E}^{b*}(\boldsymbol{r}_j)}{\boldsymbol{E}^b(\boldsymbol{r}_j)\cdot\boldsymbol{E}^{b*}(\boldsymbol{r}_j)}. \tag{17}$$

Substituting (16) into (9), we finally determine

$$\boldsymbol{E}^a_{\mathrm{QA}}(\boldsymbol{r}_j)=\boldsymbol{E}(\boldsymbol{r}_j)-\boldsymbol{E}^b(\boldsymbol{r}_j)=\int_D\hat{\boldsymbol{G}}_E(\boldsymbol{r}_j\mid\boldsymbol{r})\frac{\Delta\tilde{\sigma}(\boldsymbol{r})}{1-g(\boldsymbol{r})}\boldsymbol{E}^b(\boldsymbol{r})\,\mathrm{d}v. \tag{18}$$

A similar formula can be obtained for the magnetic field:

$$\boldsymbol{H}^a_{\mathrm{QA}}(\boldsymbol{r}_j)=\boldsymbol{H}(\boldsymbol{r}_j)-\boldsymbol{H}^b(\boldsymbol{r}_j)=\int_D\hat{\boldsymbol{G}}_H(\boldsymbol{r}_j\mid\boldsymbol{r})\frac{\Delta\tilde{\sigma}(\boldsymbol{r})}{1-g(\boldsymbol{r})}\boldsymbol{E}^b(\boldsymbol{r})\,\mathrm{d}v. \tag{19}$$

Formulae (18) and (19) give QA solutions for 3D EM fields. Note that the only difference between the new QA approximation and the Born approximation (11) is in the presence of the scalar function $[1-g(\boldsymbol{r})]^{-1}$. This is why the computational expenses to generate the QA approximation and the Born approximation are practically the same. On the other hand, it is demonstrated in Zhdanov *et al* (1999) that the accuracy of the QA approximation is much higher than the accuracy of the Born approximation.

To illustrate this fact we present the results of numerical experiments for the model shown in figure 1. It consists of a conductive rectangular prism embedded in a homogeneous half-space excited by a horizontal rectangular loop. The frequency is 1000 Hz and the conductivity ratio between the conductive prism and the homogeneous background is 10. The receivers are located above the body along the $y$-axis. Figure 2 shows the real and imaginary parts of the horizontal electric and vertical magnetic components of the scattered field computed by solving the full integral equation (SYSEM code by Xiong (1992)) and the approximate solutions. The deviations of the QA approximation from the true solution are invisible, while the Born approximation fails.

Another advantage of using expressions (18) and (19) for forward modelling is the ability to generate a simple formula for the Frechet derivative operator which can be used in inversion algorithms. For example, by introducing a perturbation of the anomalous conductivity $\delta\Delta\tilde{\sigma}(\boldsymbol{r})$ we can calculate the corresponding perturbation of the electric field $\delta\boldsymbol{E}(\boldsymbol{r}_j)$ on the basis of equation (18):

$$\delta\boldsymbol{E}(\boldsymbol{r}_j)=\int_D\hat{\boldsymbol{G}}_E(\boldsymbol{r}_j\mid\boldsymbol{r})\frac{\delta\Delta\tilde{\sigma}(\boldsymbol{r})}{1-g(\boldsymbol{r})}\boldsymbol{E}^b(\boldsymbol{r})\,\mathrm{d}v+\int_D\hat{\boldsymbol{G}}_E(\boldsymbol{r}_j\mid\boldsymbol{r})\frac{\Delta\tilde{\sigma}(\boldsymbol{r})\delta g(\boldsymbol{r})}{(1-g(\boldsymbol{r}))^2}\boldsymbol{E}^b(\boldsymbol{r})\,\mathrm{d}v, \tag{20}$$

where

$$\delta g(\boldsymbol{r})=\frac{\delta\boldsymbol{E}^B(\boldsymbol{r})\cdot\boldsymbol{E}^{b*}(\boldsymbol{r})}{\boldsymbol{E}^b(\boldsymbol{r})\cdot\boldsymbol{E}^{b*}(\boldsymbol{r})}=\int_D\hat{\boldsymbol{G}}_E(\boldsymbol{r}\mid\boldsymbol{r}')\delta\Delta\tilde{\sigma}(\boldsymbol{r}')\frac{\boldsymbol{E}^b(\boldsymbol{r}')\cdot\boldsymbol{E}^{b*}(\boldsymbol{r})}{\boldsymbol{E}^b(\boldsymbol{r})\cdot\boldsymbol{E}^{b*}(\boldsymbol{r})}\,\mathrm{d}v'. \tag{21}$$

Substituting equation (21) into the second integral in (20) and changing the notations for the integration variables, $\boldsymbol{r}\to\boldsymbol{r}'$ and $\boldsymbol{r}'\to\boldsymbol{r}$, we obtain

$$\int_D\hat{\boldsymbol{G}}_E(\boldsymbol{r}_j\mid\boldsymbol{r})\frac{\Delta\tilde{\sigma}(\boldsymbol{r})\delta g(\boldsymbol{r})}{(1-g(\boldsymbol{r}))^2}\boldsymbol{E}^b(\boldsymbol{r})\,\mathrm{d}v=\int_D\delta\Delta\tilde{\sigma}(\boldsymbol{r})\hat{\boldsymbol{K}}(\boldsymbol{r}_j\mid\boldsymbol{r})\boldsymbol{E}^b(\boldsymbol{r})\,\mathrm{d}v, \tag{22}$$

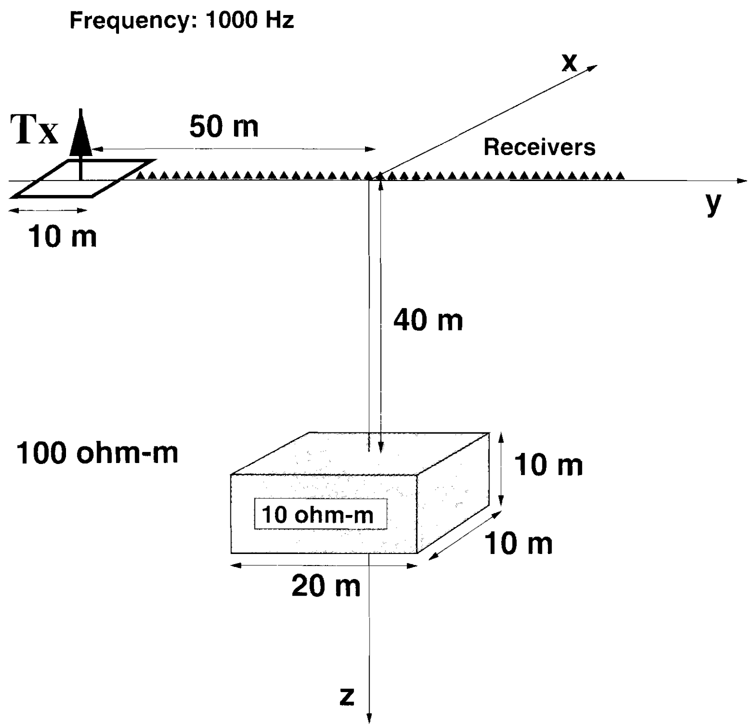


**Figure 1.** Three-dimensional geoelectrical model of rectangular conductive prism embedded in a homogeneous half-space excited by a horizontal rectangular loop.

where

$$\hat{K}(r_j \mid r) = \int_D \hat{G}_E(r_j \mid r')\hat{G}_E(r' \mid r)E^b(r')\frac{\Delta\tilde{\sigma}(r')}{(1-g(r'))^2}\frac{E^{b*}(r')}{E^b(r')\cdot E^{b*}(r')}\,\mathrm{d}v'. \tag{23}$$

Therefore,

$$\delta E(r_j) = \int_D \delta\Delta\tilde{\sigma}(r)F_E(r_j \mid r)\,\mathrm{d}v, \tag{24}$$

where the vector function $F_E(r_j \mid r)$ is the kernel of the integral Frechet derivative operator

$$F_E(r_j \mid r) = \left[\frac{1}{1-g(r)}\hat{G}_E(r_j \mid r) + \hat{K}(r_j \mid r)\right]E^b(r). \tag{25}$$

In particular, considering the infinitely small domain of the conductivity perturbation, we arrive at the following formula for the Frechet derivative of the electric field:

$$\frac{\partial E(r_j)}{\partial \Delta\tilde{\sigma}(r)} = F_E(r_j \mid r).$$

The last formula provides an analytical expression for computing the Frechet derivative matrix. Note that, in this case, the amount of calculation for the forward modelling solution and for the Frechet derivative is equivalent to computing the Born approximation.

## 3. Inversion based on the QA method

An EM inverse problem, in a general case, can be described by an operator equation

$$d = G(m), \tag{26}$$

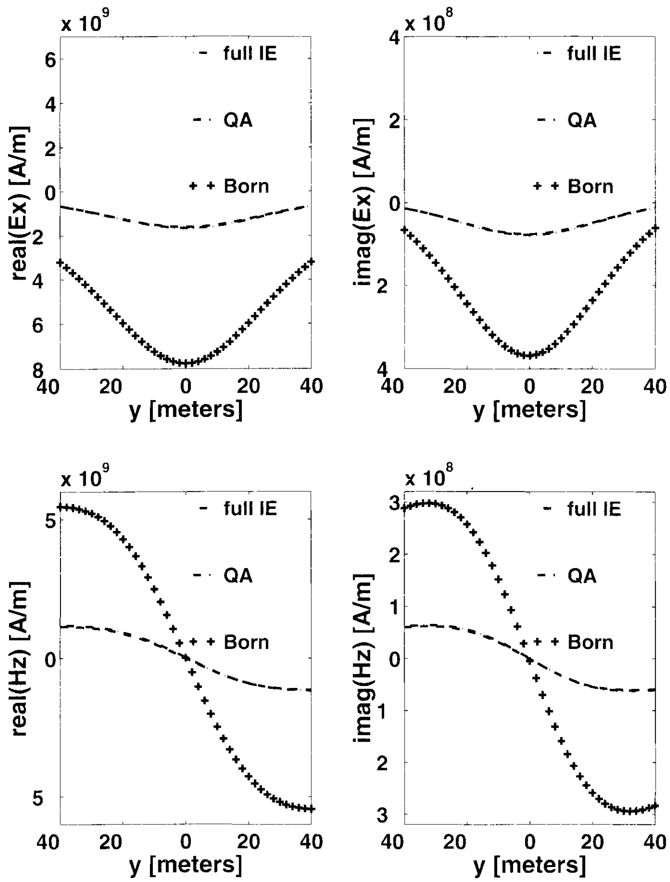


**Figure 2.** Behaviour of the anomalous horizontal electric and vertical magnetic field components computed for the model in the previous figure by solving the full integral equation, Born approximation and the QA approximations.

where $\boldsymbol{G}$ is a forward modelling operator, $\boldsymbol{m}$ stands for a set of the model parameters describing the anomalous conductivity distribution, $\Delta\tilde{\sigma}$, and $\boldsymbol{d}$ is an EM data set. Using a discrete formula, derived in appendix A, we can rewrite equation (26) in the form

$$\boldsymbol{d} = \boldsymbol{G}(\boldsymbol{m}) = \hat{\boldsymbol{A}}[\mathrm{diag}(\boldsymbol{I} - \hat{\boldsymbol{C}}\boldsymbol{m})]^{-1}\boldsymbol{m}, \tag{27}$$

where $\boldsymbol{I}$ is a column vector formed by units and $\hat{\boldsymbol{A}}$ stands for electric or magnetic matrices, respectively:

$$\hat{\boldsymbol{A}}_E = \hat{\boldsymbol{G}}_E \hat{e}^b \qquad \text{or} \qquad \hat{\boldsymbol{A}}_E = \hat{\boldsymbol{G}}_E \hat{e}^b, \tag{28}$$

matrix $\hat{\boldsymbol{C}}$ depends on the matrix of the background electric field $\hat{e}^b$, introduced in appendix A (formula (57)),

$$\hat{\boldsymbol{C}} = (\hat{e}^b \hat{e}^{b*})^{-1} \hat{e}^{b*} \hat{\boldsymbol{G}}_D \hat{e}^b, \tag{29}$$

and $\mathrm{diag}(\boldsymbol{I} - \hat{\boldsymbol{C}}\boldsymbol{m})$ is a diagonal matrix determined by the model parameters $\boldsymbol{m}$ (anomalous conductivity distribution, $\Delta\tilde{\sigma}$).

The remarkable fact is that the full matrices $\hat{\boldsymbol{A}}$ and $\hat{\boldsymbol{C}}$ in the discrete form of the QA approximation are independent of the anomalous conductivity. Therefore, formula (27) is very efficient in iterative inversion because these matrices have to be precomputed only once for the entire inverse process. Note that the Green functions are computed using the Fast Hankel Transform (Xiong 1992). The only term depending on the model parameters $\boldsymbol{m}$ is the diagonal matrix diag$(\boldsymbol{I} - \hat{\boldsymbol{C}}\boldsymbol{m})$, which is easy to compute for a given $\hat{\boldsymbol{C}}$. These results make QA approximation a very powerful tool in inversion.

Inverse problem (26) is usually ill-posed, i.e. the solution can be non-unique and unstable. The conventional way of solving ill-posed inverse problems, according to regularization theory (Tikhonov and Arsenin 1977, Zhdanov 1993), is based on minimization of the Tikhonov parametric functional:

$$P^{\alpha}(\boldsymbol{m}) = \varphi(\boldsymbol{m}) + \alpha s(\boldsymbol{m}), \tag{30}$$

where $\varphi(\boldsymbol{m})$ is a misfit functional between the theoretical values $\boldsymbol{G}(\boldsymbol{m})$ and the observed data $\boldsymbol{d}$, $s(\boldsymbol{m})$ is a stabilizing functional and $\alpha$ is a regularization parameter. The optimal value of $\alpha$ is determined from the misfit condition

$$\varphi(\boldsymbol{m}) = \delta_d, \tag{31}$$

where $\delta_d$ is the noise level of the data.

The minimization problem (30) can be solved using any gradient type technique, say, by the conjugate gradient (CG) method. The critical point of an inversion algorithm is the calculation of the Frechet derivative (sensitivity) operator $\boldsymbol{F}$ at every iteration of the CG method. The QA solutions described above provide a very effective and elegant way to compute directly the Frechet derivative (sensitivity matrix), outlined in appendix A:

$$\delta \boldsymbol{d} = \hat{\boldsymbol{F}}(\boldsymbol{m})\delta \boldsymbol{m},$$

where

$$\hat{\boldsymbol{F}}(\boldsymbol{m}) = \hat{\boldsymbol{A}}\{\hat{\boldsymbol{B}}(\boldsymbol{m}) + \mathrm{diag}(\boldsymbol{m})\hat{\boldsymbol{B}}^2(\boldsymbol{m})\hat{\boldsymbol{C}}\} \tag{32}$$

$$\hat{\boldsymbol{B}}(\boldsymbol{m}) = [\mathrm{diag}(\boldsymbol{I} - \hat{\boldsymbol{C}}\boldsymbol{m})]^{-1} \tag{33}$$

and diag$(\boldsymbol{m})$ denotes a diagonal matrix formed by the elements of the vector $\boldsymbol{m}$.

Note again that numerical computations based on formula (32) are very fast and efficient because the full matrices $\hat{\boldsymbol{A}}$ and $\hat{\boldsymbol{C}}$ are precomputed for the background model and are fixed; we update only the diagonal matrix $\hat{\boldsymbol{B}}(\boldsymbol{m})$ on each iteration of the inverse process.

## 4. Principles of imaging geological structures with sharp geoelectrical boundaries

According to the basic principles of the regularization method, we have to find the model $\boldsymbol{m}_{\alpha}$, a quasi-solution of the inverse problem (26), that minimizes the parametric functional (30)

$$P^{\alpha}(\boldsymbol{m}) = \min. \tag{34}$$

Usually, the misfit functional is specified as

$$\phi(\boldsymbol{m}) = \|\hat{\boldsymbol{W}}_d(\boldsymbol{G}(\boldsymbol{m}) - \boldsymbol{d})\|^2 = (\boldsymbol{G}(\boldsymbol{m}) - \boldsymbol{d})^* \hat{\boldsymbol{W}}_d^2 (\boldsymbol{G}(\boldsymbol{m}) - \boldsymbol{d}), \tag{35}$$

where $\boldsymbol{W}_d$ is some weighting matrix of data and symbol '*' means transposed complex conjugated matrix.

There are several common choices for stabilizers in the parametric functional (30). One is based on the least squares criterion. Another stabilizer uses a minimum norm of difference between the selected model and some *a priori* model. For example, the stabilizer may be selected to be equal to

$$s(\boldsymbol{m}) = \|\hat{\boldsymbol{W}}_m(\boldsymbol{m} - \boldsymbol{m}_{\mathrm{apr}})^2\| = (\boldsymbol{m} - \boldsymbol{m}_{\mathrm{apr}})^* \hat{\boldsymbol{W}}_m^2 (\boldsymbol{m} - \boldsymbol{m}_{\mathrm{apr}}), \tag{36}$$

where $\hat{W}_m$ is some weighting matrix of model parameters and $m_{\rm apr}$ is some *a priori* reference model, selected on the basis of all available geological and geophysical information about the area under investigation. The solution of the minimization problem (34) with the misfit and stabilizing functionals, determined by equations (35) and (36), can be obtained by the regularized conjugate gradient (RCG) method (see appendix B).

The stabilizer (36) applied to the gradient of the model parameters brings us to a maximum smoothness stabilizing functional. It has been successfully used in many inversion schemes developed for EM data interpretation (Berdichevsky and Zhdanov 1984, Constable *et al* 1987, Smith and Booker 1991, Zhdanov and Fang 1996b). This stabilizer produces smooth models, which in many practical situations does not describe properly the real blocky geological structures.

In Portniaguine and Zhdanov (1999), another stabilizing functional was considered which minimized the area of the anomalous conductivity distribution. This functional was called a minimum support (MS) functional.

The MS functional can be described as follows. Consider the following integral of the model parameter distribution:

$$J_\beta(m) = \int_V \frac{m^2}{m^2 + \varepsilon^2}\,\mathrm{d}v. \tag{37}$$

We introduce the support of $m$ (denoted spt$m$) as the combined closed subdomains of $V$ where $m \neq 0$. We call spt$m$ a model parameter support. Then expression (37) can be modified:

$$J_\varepsilon(m) = \int_{\mathrm{spt}m}\left[1 - \frac{\varepsilon^2}{m^2+\varepsilon^2}\right]\mathrm{d}v = \mathrm{spt}m - \varepsilon^2\int_{\mathrm{spt}m}\frac{1}{m^2+\varepsilon^2}\,\mathrm{d}v. \tag{38}$$

From the last expression we can see that

$$J_\varepsilon(m) \to \mathrm{spt}m, \qquad \text{if} \quad \varepsilon \to 0. \tag{39}$$

Thus, integral $J_\varepsilon(m)$ can be treated as a functional, proportional (for a small $\varepsilon$ ) to the model parameter support. We can use this integral to introduce a MS stabilizing functional $s_{\rm MS}(m)$ as follows:

$$s_{\rm MS}(m) = J_\varepsilon(m - m_{\rm apr}) = \int_V \frac{(m-m_{\rm apr})^2}{(m-m_{\rm apr})^2+\varepsilon^2}\,\mathrm{d}v. \tag{40}$$

It is proved in Portniaguine and Zhdanov (1999) that the MS functional satisfies the Tikhonov criterion for a stabilizer. For discrete model parameters $\boldsymbol{m}$, functional $s_{\rm MS}$ can be written using matrix notations

$$s_{\rm MS}(\boldsymbol{m}) = (\boldsymbol{m} - \boldsymbol{m}_{\rm apr})^*(\mathrm{diag}[(\boldsymbol{m} - \boldsymbol{m}_{\rm apr})^2 + \varepsilon^2])^{-1}(\boldsymbol{m} - \boldsymbol{m}_{\rm apr}). \tag{41}$$

We can introduce a variable diagonal weighting matrix $\hat{W}_e(\boldsymbol{m})$ according to the formula

$$\hat{W}_e(\boldsymbol{m}) = \mathrm{diag}[(\boldsymbol{m} - \boldsymbol{m}_{\rm apr})^2 + \varepsilon^2]^{1/2}. \tag{42}$$

Then the stabilizing functional can be written as the weighted least square norm of the model parameters

$$s_{\rm MS}(\boldsymbol{m}) = (\boldsymbol{m} - \boldsymbol{m}_{\rm apr})^*\hat{W}_e^{-2}(\boldsymbol{m} - \boldsymbol{m}_{\rm apr}). \tag{43}$$

Note that it is still important to use in the inversion scheme the permanent weights of model parameters $\hat{W}_m$ introduced in the original stabilizer (36). The fact is that the sensitivity of the data to the different model parameters is different because the contribution of the different parameters in the observation is also different. For example, the effect of the shallow parts of the geoelectrical cross-section is much more significant than the effect of the deep structures.

The weighting matrix $\hat{W}_m$ can be constructed in such a way that the sensitivity of the data to the weighted model parameters will become more or less equal. We have demonstrated in Mehanee and Zhdanov (1998) that the matrix $\hat{W}_m$ with this property can be determined as the square root of the integrated Frechet derivative (sensitivity) matrix:

$$\hat{W}_m = \sqrt{\hat{S}}, \tag{44}$$

where $\hat{S}$ is the diagonal matrix formed by the integrated sensitivities of the field data $d$ to the parameter $m_k$, determined as the ratio

$$S_k = \frac{\|\delta d\|}{\delta m_k} = \sqrt{\sum_i (F_{ik})^2}. \tag{45}$$

In the last formula $F_{ik}$ are the elements of the Frechet derivative matrix $\hat{F}(m_0)$ for the initial model.

In a similar way, we can define the data-weighting matrix as

$$W_d = \operatorname{diag}\left(4\sqrt{\sum_k (F_{i\bar{k}})^2}\right). \tag{46}$$

These weights make normalized data less dependent on the frequency and distance from the anomalous domain, which improves the resolution of the inverse method.

The parametric functional we seek to minimize can be written using matrix notations:

$$P^{\alpha}(m) = (G(m) - d)^* \hat{W}_d^2 (G(m) - d) + \alpha (m - m_{\mathrm{apr}})^* \hat{W}_e^{-2} \hat{W}_m^2 (m - m_{\mathrm{apr}}) = \min . \tag{47}$$

Note that in this case we implement the MS functional by introducing the variable weighting matrix $\hat{W}_e$. Therefore, the problem of the minimization of the parametric functional introduced by equation (47) can be treated in a similar way to the minimization of the conventional Tikhonov functional with the least square stabilizer (36). The only difference is that now we introduce some variable weighting matrix, $\hat{W}_e$, for model parameters. This method is similar to the variable metric method. However, in our case, the variable weighted metric is used in calculation of the stabilizing functional only.

The minimization of the parametric functional (47) can be carried out using the CG method similar to one outlined in appendix B. Numerical calculations, however, demonstrate that the most efficient way to solve this problem is based on minimization in the space of weighted parameters. We will discuss the basic ideas of this method in the next section.

## 5. Minimization in the space of weighted parameters

The minimization problem (47) can be reformulated using the space of weighted parameters:

$$m^w = \hat{W}_e^{-1} \hat{W}_m m. \tag{48}$$

We introduce also the weighted data

$$d^w = \hat{W}_d d. \tag{49}$$

We can consider the forward operator, which relates the new weighted parameters $m^w$ to the weighted data,

$$d^w = G^w(m^w) = \hat{W}_d G(\hat{W}_m^{-1} \hat{W}_e m^w). \tag{50}$$

Note that from formula (50), we obtain a simple relationship between the Frechet derivative matrices of the new, $G^w(m^w)$, and old, $G(m)$, forward modelling operators:

$$\delta G^w(m^w) = \hat{F}_w \delta m^w = \hat{W}_d \delta G \hat{W}_m^{-1} \hat{W}_e m^w.$$

Therefore,

$$\hat{F}_w = \hat{W}_d \hat{F} \hat{W}_m^{-1} \hat{W}_e. \tag{51}$$

Using these notations we can rewrite the parametric functional (47) as follows:

$$P^{\alpha}(m^{w}) = (G^{w}(m^{w}) - d^{w})^{*}(G^{w}(m^{w}) - d^{w}) + \alpha(m^{w} - m^{w}_{\mathrm{apr}})^{*}(m^{w} - m^{w}_{\mathrm{apr}}) = \min . \tag{52}$$

Note that the unknown parameters now are weighted model parameters $m^{w}$. In order to obtain the original conductivity distribution we have to apply inverse weighting to the result of the minimization of the parametric functional (52):

$$m = \hat{W}_m^{-1} \hat{W}_e m^{w}. \tag{53}$$

The numerical experiments show that, as a rule, the iterative process converges faster for (52) than for (47). The minimization method in the space of weighted parameters is similar to the RCG method described in appendix B. One can find a detailed description of the re-weighted RCG method in the space of weighted parameters in appendix C.

## 6. Model studies

### *6.1. Model 1*

Consider a homogeneous half-space with resistivity of 100 $\Omega$ m, containing a conductive inhomogeneous body. The resistivity of the inhomogeneity is 16 $\Omega$ m. The anomalous body represents a tilted dyke structure. The top of the anomaly is 200 m and its bottom is 500 m beneath the surface. This model is excited by an electric current bipole with 500 m electrode separation. The source is located 2000 m from the centre of the inhomogeneity. The source has been fed by alternating currents with five different frequencies: 0.1, 1, 10, 100 and 1000 Hz. The $x$, $y$ and $z$ components of the anomalous magnetic field have been simulated at nine receiver points arranged on a homogeneous grid. The $x$ and $y$ coordinates of the receiver grid are $x = y = -250$, 0 and 250 m. Both the source and the receiver system are located at the surface of the earth. The sketch of the model and the measuring system is shown in figure 3. The inverted area is a homogeneous mesh consisting of $6 \times 6 \times 6$ cubic cells surrounding the anomalous structure to be inverted. Each cell has a dimension of 100 m in the $x$, $y$ and $z$ directions. Note that in this case the cell size is comparable with the skin depth for the highest frequency. For better resolution of the inversion one should consider the finer discretization. However, in our case, even this rough discretization works reasonably well, as we will see from the numerical results of the inversion. The inverted area is also shown in figure 3. The vertical slices of the inverted area and the true model are presented in figure 4.

The data vector consists of 135 simulated field components. The synthetic data is generated by a full integral equation code and it has been contaminated by 3% random noise. The model parameters are the unknown anomalous conductivity values of each cell of the inverted area.

The inversion problem is ill-posed and underdetermined, so we use the RCG method described above in this paper. We performed Born and QA inversions using smooth (minimum norm) and sharp (MS) stabilizers.

The results of the Born and QA inversions using smooth stabilizer are shown in figures 5 and 6. As we can expect, we obtain an image which has spread around the location of the inhomogeneity. The conductivity contrast is underestimated. It is very difficult to recognize the dyke in the image obtained by the smooth Born inversion. The inverse image generated by the smooth QA inversion resolves slightly better the inclined dyke. However, the image is still diffuse and unclear.

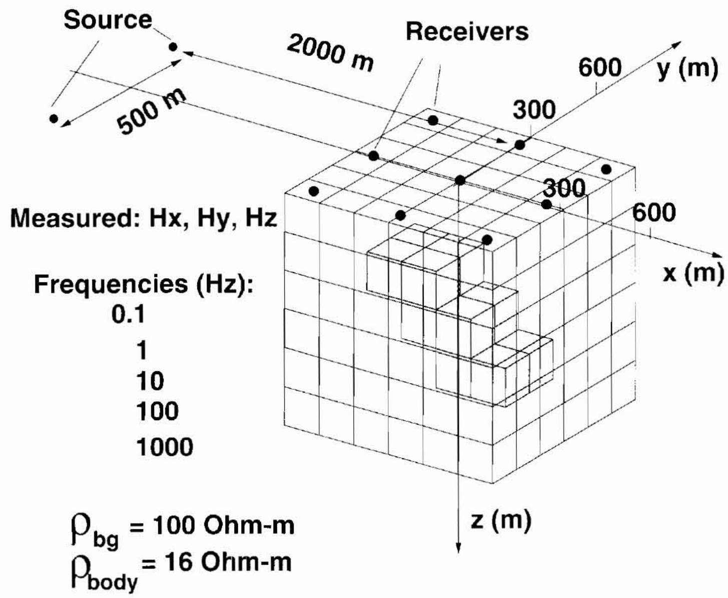


**Figure 3.** Three-dimensional geoelectrical model of a tilted conductive dyke embedded in a homogeneous half-space excited by a horizontal electric bipole (model 1). The discretization of the inverted area is also shown. The receivers are marked by dots right above the inverted area.

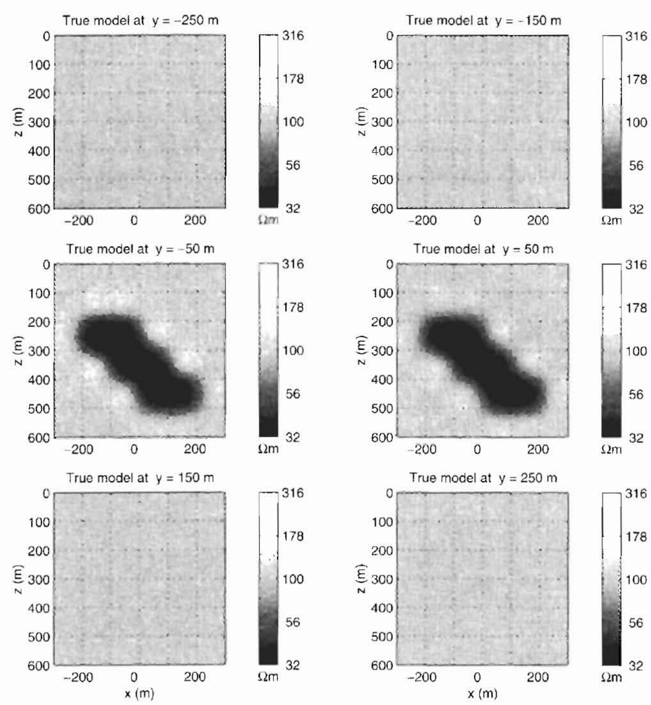


**Figure 4.** Vertical cross-sections of the inverted area and the true model for model 1. Dotted lines mark the discretization of the inverted area.

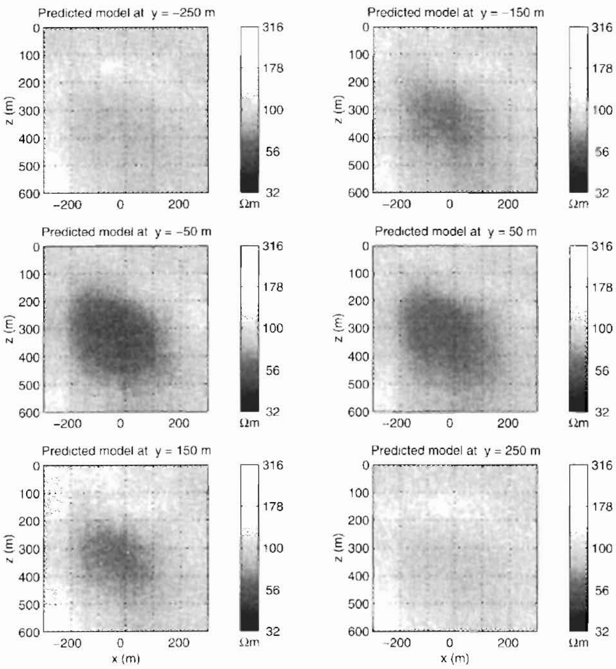


**Figure 5.** Vertical cross-sections of the predicted model for model 1 after smooth Born inversion. Dotted lines mark the discretization of the inverted area.

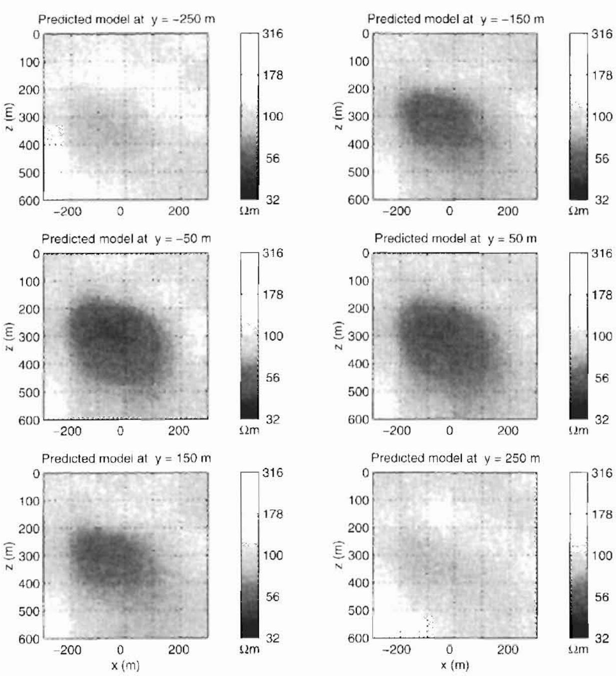


**Figure 6.** Vertical cross-sections of the predicted model for model 1 after smooth QA inversion. Dotted lines mark the discretization of the inverted area.

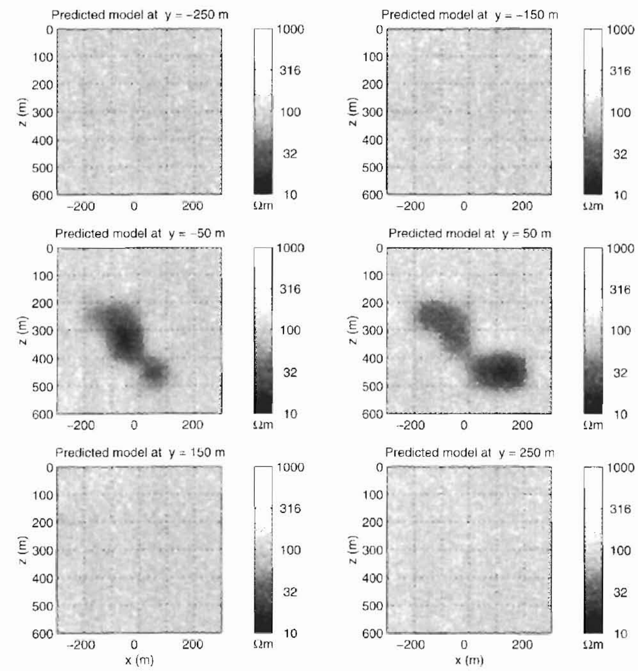


**Figure 7.** Vertical cross-sections of the predicted model for model 1 after sharp Born inversion. Dotted lines mark the discretization of the inverted area.

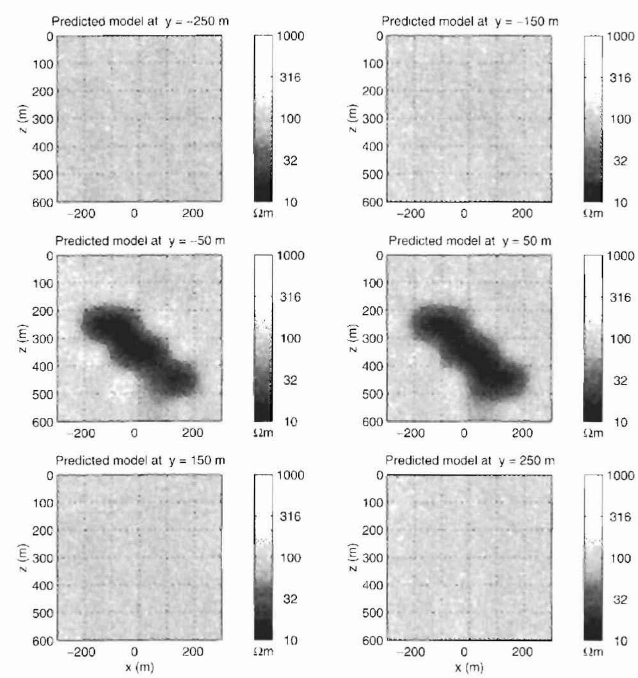


**Figure 8.** Vertical cross-sections of the predicted model for model 1 after sharp QA inversion. Dotted lines mark the discretization of the inverted area.

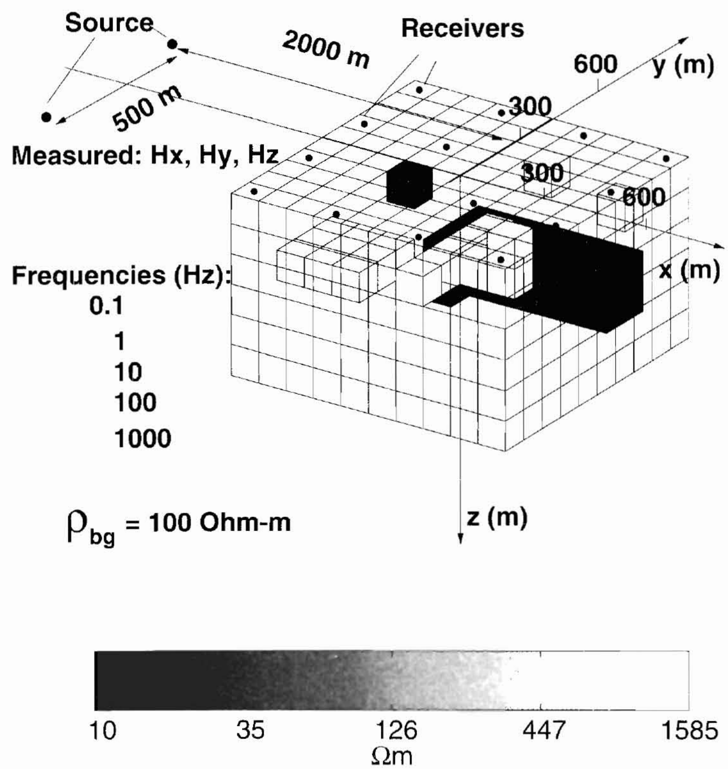


**Figure 9.** Three-dimensional geoelectrical model of several conductive and resistive bodies embedded in a homogeneous half-space excited by a horizontal electric bipole (model 2). The discretization of the inverted area is also shown. The receivers are marked by dots right above the inverted area.

The difference between the QA and Born inversion becomes significant if we use the sharp stabilizer. If we have a good estimation of the upper and lower boundaries of the model parameters, using this stabilizer we can usually recover the geometry of the anomalous structure with high resolution. Also, this requires a very accurate forward modelling as a basis for the inversion. The sharp Born inversion gives an underestimated size of the anomaly (figure 7). The physical explanation for this is that, in the case of conductive anomalies, the Born approximation gives higher field values than the exact solution. Therefore, an inversion based on this will underestimate the conductance of the anomaly, which corresponds to a smaller size for the given conductivity.

The QA inversion solves this problem. It is based on a much more accurate forward operator than the Born approximation. The difference between the synthetic data computed by the QA approximation and full integral equation (IE) solution is less than the given noise level. Therefore, the QA inversion provides almost perfect reconstruction of the given model (figure 8).

With a reasonable estimate of the noise level, the stopping criteria of the inversion can be assigned to the point where the relative misfit is minimized to this error level. In our case, it was 3%. The re-weighting in the sharp inversion causes an increment of the misfit. We re-weight again only if the misfit drops to the given noise level or if the parametric functional increases due to the penalization.

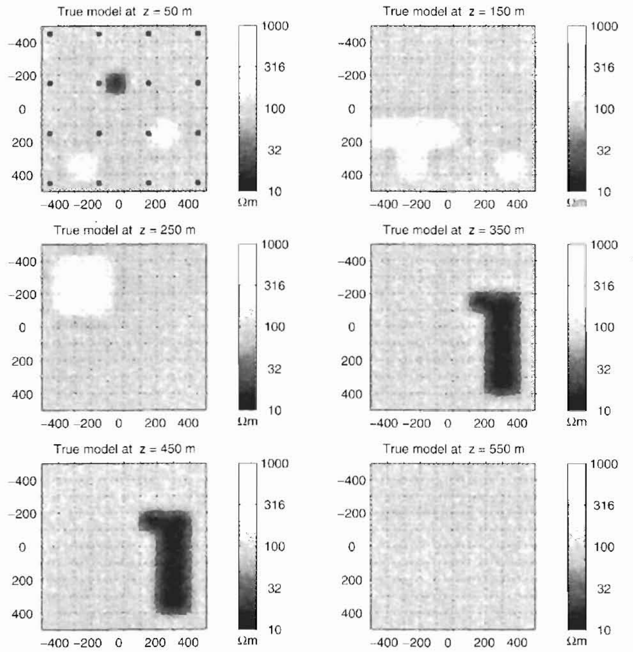


**Figure 10.** Horizontal cross-sections of the inverted area and the true model for model 2. Dots show the location of receiver points. Dotted lines mark the discretization of the inverted area.

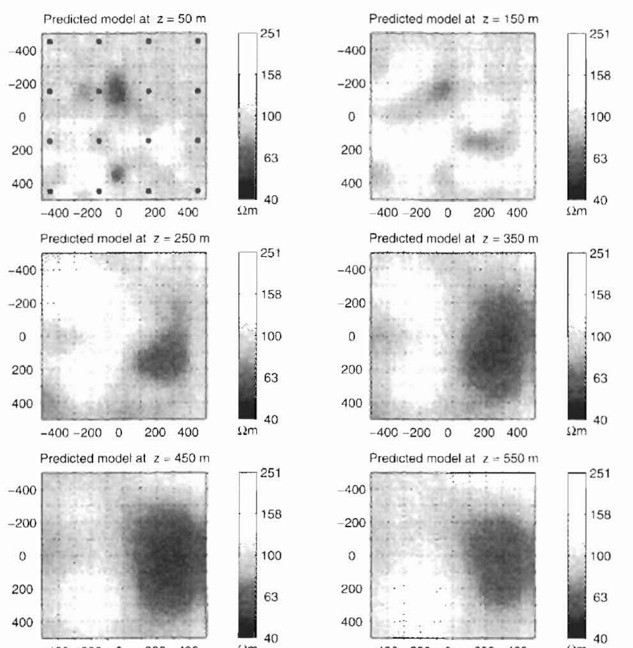


**Figure 11.** Horizontal cross-sections of the predicted model for model 2 after smooth Born inversion. Dots show the location of receiver points. Dotted lines mark the discretization of the inverted area.

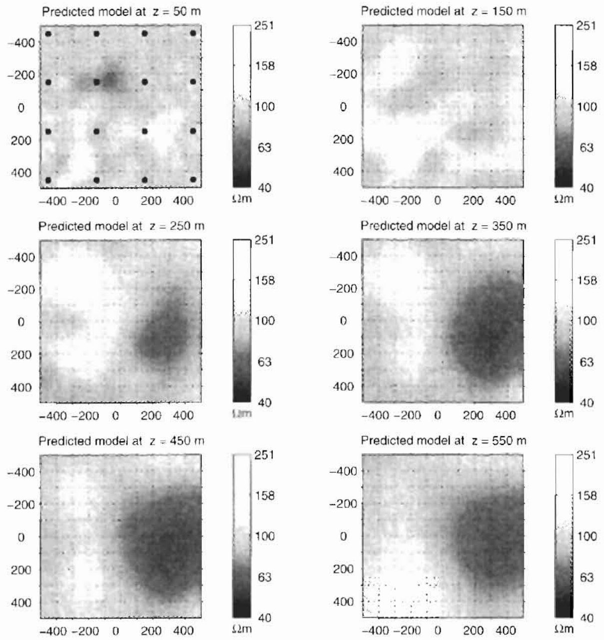


**Figure 12.** Horizontal cross-sections of the predicted model for model 2 after smooth QA inversion. Dots show the location of receiver points. Dotted lines mark the discretization of the inverted area.

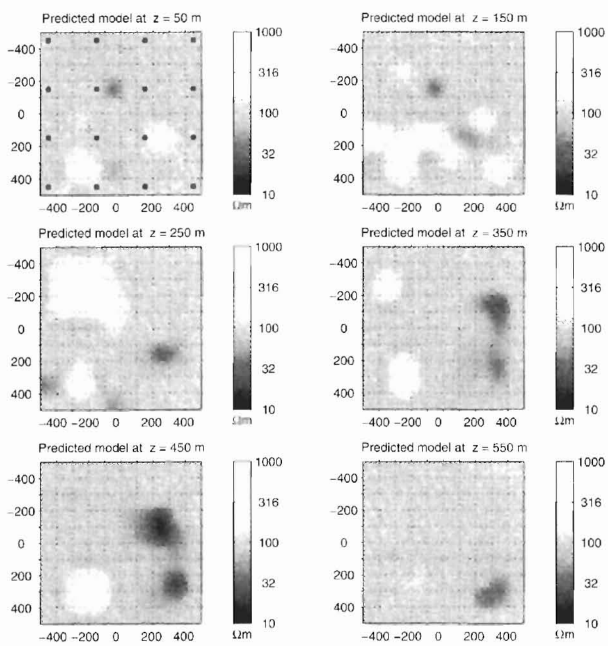


**Figure 13.** Horizontal cross-sections of the predicted model for model 2 after sharp Born inversion. Dots show the location of receiver points. Dotted lines mark the discretization of the inverted area.

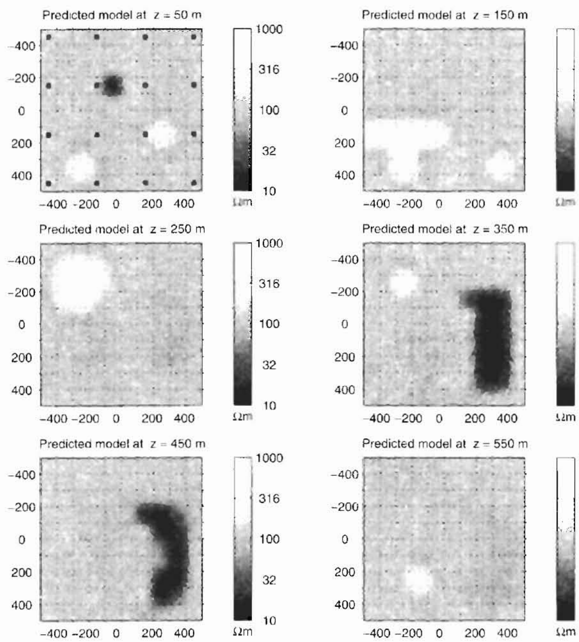


**Figure 14.** Horizontal cross-sections of the predicted model for model 2 after sharp QA inversion. Dots show the location of receiver points. Dotted lines mark the discretization of the inverted area.

### *6.2. Model 2*

This model represents a more complicated structure with several resistive and conductive bodies. The background model and the source are exactly the same as in model 1. The frequencies are 0.1, 1, 10, 100 and 1000 Hz. In this experiment, as in model 1, we simulated the three components of the anomalous magnetic field by solving a full IE, and the data was contaminated by 3% random noise.

The receivers are located on a $4 \times 4$ grid with $x = y = -450, -150, 150$ and $450$ m coordinates at the surface ($z = 0$). The inverted area has been discretized by $10 \times 10 \times 6$ cubic cells of 100 m size in the $x$, $y$ and $z$ directions.

The 3D picture of the model and the measurement system with the inverted area is presented in figure 9. Figure 10 provides horizontal slices giving a more detailed image of the model.

Similarly to the previous model study, we performed Born and QA inversions using smooth and sharp stabilizers.

This problem is even more underdetermined than the previous one, therefore the resolution of smooth inversions is poor. We obtain large smooth patches with underestimated conductivity contrasts with the Born inversion (figure 11) and a slightly better image with QA inversion figure (12).

If we use a focusing inversion algorithm, then we can obtain much more realistic models for both cases. However, the Born inversion gives a large number of unwanted artifacts, overestimated resistive and underestimated conductive structures (figure 13). Most of these deviations disappear using the QA inversion technique (figure 14). We can see that even such a complicated 3D model can be reconstructed based on a relatively small amount of data.

## 7. Conclusions

We have presented a new method of 3D EM inversion based on fast and accurate QA approximations for both the forward modelling operator and the Frechet derivative. The remarkable property of this approximation is that updating the Frechet derivative matrix for different iterations requires computing the diagonal matrices only. Therefore, the numerical computations based on the QA approximation are very fast and efficient.

The developed inverse method uses the ideas of regularization and image focusing. Using a model study, we demonstrate that QA inversion with focusing provides a sharp and clear image of rather complicated 3D targets.

The future directions for research will include implementation of the more accurate reflectivity tensor approximations in the QA inversion code, which were introduced in Zhdanov *et al* (1999), and applying the code to practical data sets.

## Acknowledgments

Financial support for this work was provided by the National Science Foundation under the grant No ECS-9987779. The authors also acknowledge the support of the University of Utah Consortium for EM Modelling and Inversion (CEMI), which includes Advanced Power Technologies Inc., AGIP, Baker Atlas Logging Services, BHP Minerals, EXXON-MOBIL Upstream Research Company, Geological Survey of Japan, INCO Exploration, Japan National Oil Corporation, MINDECO, Naval Research Laboratory, Rio Tinto-Kennecott, 3JTech Corporation and Zonge Engineering.

## Appendix A. QA approximation in numerical dressing; Frechet derivative matrix

In practice, we usually solve forward and inverse problems in the space of discrete data and model parameters. Suppose that $M$ measurements of an electric or magnetic field are performed in some EM experiment. Then we can consider these values as the components of electric, $\boldsymbol{e}$, or magnetic, $\boldsymbol{h}$, vectors of a length $3M$:

$$\boldsymbol{e} = [E_x^1, E_x^1, \ldots, E_x^M, E_y^1, E_y^1, \ldots, E_y^M, E_z^1, E_z^1, \ldots, E_z^M]^T,$$

$$\boldsymbol{h} = [H_x^1, H_x^1, \ldots, H_x^M, H_y^1, H_y^1, \ldots, H_y^M, H_z^1, H_z^1, \ldots, H_z^M]^T,$$

where the upper subscript '$T$' denotes a transpose operation of a vector row into a vector column.

Similarly, anomalous conductivity distribution, $\Delta\tilde{\sigma}(\boldsymbol{r})$, on some grid can be represented as the components of a vector $\boldsymbol{m}$ of the length $N$:

$$\boldsymbol{m} = [m_1, m_2, \ldots, m_N]^T = [\Delta\tilde{\sigma}_1, \Delta\tilde{\sigma}_2, \ldots, \Delta\tilde{\sigma}_N]^T.$$

Using these notations, we can write the discrete analogues of the Born approximation (11) and QA approximations (18) and (19) as

$$\boldsymbol{e}^B = \hat{\boldsymbol{G}}_E \hat{e}^b \boldsymbol{m}, \tag{54}$$

$$\boldsymbol{e}^a = \hat{\boldsymbol{G}}_E \hat{e}^b [\mathrm{diag}(\boldsymbol{I} - \boldsymbol{g}(\boldsymbol{m}))]^{-1}\, \boldsymbol{m} \tag{55}$$

and

$$\boldsymbol{h}^a = \hat{\boldsymbol{G}}_H \hat{e}^b [\mathrm{diag}(\boldsymbol{I} - \boldsymbol{g}(\boldsymbol{m}))]^{-1} \boldsymbol{m}. \tag{56}$$

We use the following notations in the last formulae. The vectors $\boldsymbol{e}^B$, $\boldsymbol{e}^a$ and $\boldsymbol{h}^a$ represent the discrete Born and QA approximations of the anomalous electric field at the observation points.

Matrix $\hat{e}^b$ is a sparse tri-diagonal $3N \times N$ matrix containing the $x$, $y$ and $z$ components of the primary (background) electric field at the centres of the cells of the anomalous domain $D$:

$$\hat{e}^b = \begin{bmatrix} E_x^{b,1} & & \\ & \ddots & \\ & & E_x^{b,N} \\ E_y^{b,1} & & \\ & \ddots & \\ & & E_y^{b,N} \\ E_z^{b,1} & & \\ & \ddots & \\ & & E_z^{b,N} \end{bmatrix}. \tag{57}$$

Matrices $\hat{\boldsymbol{G}}_E$ and $\hat{\boldsymbol{G}}_H$ are discrete analogues of the corresponding Green tensors. These matrices consist of the elements of either the electric or the magnetic Green tensor acting from the anomalous body to the receivers. $M$ is the number of receivers and $N$ is the number of cells in the anomalous body. The number of rows in $\hat{\boldsymbol{G}}_{E,H}$ equals the length of the data vector; $\hat{\boldsymbol{G}}_{E,H}$ has $3N$ columns:

$$\hat{\boldsymbol{G}}_{E,H} = \begin{bmatrix} G_{xx}^{11} & \cdots & G_{xx}^{1N} & G_{xy}^{11} & \cdots & G_{xy}^{1N} & G_{xz}^{11} & \cdots & G_{xz}^{1N} \\ & & & & \vdots & & & & \\ G_{xx}^{M1} & \cdots & G_{xx}^{MN} & G_{xy}^{M1} & \cdots & G_{xy}^{MN} & G_{xz}^{M1} & \cdots & G_{xz}^{MN} \\ G_{yx}^{11} & \cdots & G_{yx}^{1N} & G_{yy}^{11} & \cdots & G_{yy}^{1N} & G_{yz}^{11} & \cdots & G_{yz}^{1N} \\ & & & & \vdots & & & & \\ G_{yx}^{M1} & \cdots & G_{yx}^{MN} & G_{yy}^{M1} & \cdots & G_{yy}^{MN} & G_{yz}^{M1} & \cdots & G_{yz}^{MN} \\ G_{zx}^{11} & \cdots & G_{zx}^{1N} & G_{zy}^{11} & \cdots & G_{zy}^{1N} & G_{zz}^{11} & \cdots & G_{zz}^{1N} \\ & & & & \vdots & & & & \\ G_{zx}^{M1} & \cdots & G_{zx}^{MN} & G_{zy}^{M1} & \cdots & G_{zy}^{MN} & G_{zz}^{M1} & \cdots & G_{zz}^{MN} \end{bmatrix}.$$

Vector $\boldsymbol{I}$ is a column vector of the length $N$ formed by units. The column vector $\boldsymbol{g}(\boldsymbol{m})$ of a length $N$ represents a function $g(\boldsymbol{r})$ (equation (17)) at the centre of each cell:

$$\boldsymbol{g}(\boldsymbol{m}) = \left[ \frac{\boldsymbol{E}^{b,1*} \cdot \boldsymbol{E}^{B,1}}{\boldsymbol{E}^{b,1*} \cdot \boldsymbol{E}^{b,1}}, \frac{\boldsymbol{E}^{b,2*} \cdot \boldsymbol{E}^{B,2}}{\boldsymbol{E}^{b,2*} \cdot \boldsymbol{E}^{b,2}}, \ldots, \frac{\boldsymbol{E}^{b,N*} \cdot \boldsymbol{E}^{B,N}}{\boldsymbol{E}^{b,N*} \cdot \boldsymbol{E}^{b,N}} \right]^T, \tag{58}$$

where $\boldsymbol{E}^{B,j}$ and $\boldsymbol{E}^{b,j}$ $(j = 1, 2, \ldots, N)$ denote the Born approximation and the background electric field in each cell within the anomalous domain.

Direct calculations show that vector $\boldsymbol{g}(\boldsymbol{m})$ can be expressed by matrix multiplication:

$$\boldsymbol{g}(\boldsymbol{m}) = (\hat{e}^b \hat{e}^{b*})^{-1} \hat{e}^{b*} \boldsymbol{e}_D^B, \tag{59}$$

where the vector of the Born approximation inside the anomalous domain, $\boldsymbol{e}_D^B$, can be expressed by a formula similar to (54):

$$\boldsymbol{e}_D^B = \hat{\boldsymbol{G}}_D \hat{e}^b \boldsymbol{m}. \tag{60}$$

Matrix $\hat{\boldsymbol{G}}_D$ is a discrete analogue of the corresponding electric Green tensor acting inside the domain $D$. It is the $3N \times 3N$ scattering matrix consisting of the elements of the electric Green tensor inside the anomalous domain:

$$\hat{G}_D = \begin{bmatrix} G_{xx}^{11} & \cdots & G_{xx}^{1N} & G_{xy}^{11} & \cdots & G_{xy}^{1N} & G_{xz}^{11} & \cdots & G_{xz}^{1N} \\ & & & & \vdots & & & & \\ G_{xx}^{N1} & \cdots & G_{xx}^{NN} & G_{xy}^{N1} & \cdots & G_{xy}^{NN} & G_{xz}^{N1} & \cdots & G_{xz}^{NN} \\ G_{yx}^{11} & \cdots & G_{yx}^{1N} & G_{yy}^{11} & \cdots & G_{yy}^{1N} & G_{yz}^{11} & \cdots & G_{yz}^{1N} \\ & & & & \vdots & & & & \\ G_{yx}^{N1} & \cdots & G_{yx}^{NN} & G_{yy}^{N1} & \cdots & G_{yy}^{NN} & G_{yz}^{N1} & \cdots & G_{yz}^{NN} \\ G_{zx}^{11} & \cdots & G_{zx}^{1N} & G_{zy}^{11} & \cdots & G_{zy}^{1N} & G_{zz}^{11} & \cdots & G_{zz}^{1N} \\ & & & & \vdots & & & & \\ G_{zx}^{N1} & \cdots & G_{zx}^{NN} & G_{zy}^{N1} & \cdots & G_{zy}^{NN} & G_{zz}^{N1} & \cdots & G_{zz}^{NN} \end{bmatrix}.$$

Substituting (60) into (59) we obtain

$$g(\boldsymbol{m}) = (\hat{e}^b\hat{e}^{b*})^{-1}\hat{e}^{b*}\boldsymbol{e}^B = (\hat{e}^b\hat{e}^{b*})^{-1}\hat{e}^{b*}\hat{\boldsymbol{G}}_D\hat{e}^b\boldsymbol{m} = \hat{\boldsymbol{C}}\boldsymbol{m}, \tag{61}$$

where

$$\hat{C} = (\hat{e}^b\hat{e}^{b*})^{-1}\hat{e}^{b*}\hat{\boldsymbol{G}}_D\hat{e}^b. \tag{62}$$

Thus, we can represent equations (54)–(56) in the form

$$\begin{aligned} \boldsymbol{e}^B &= \hat{\boldsymbol{G}}_E\hat{e}^b\boldsymbol{m} = \hat{\boldsymbol{A}}_E\boldsymbol{m} \\ \boldsymbol{e}^a_{\mathrm{QA}} &= \hat{\boldsymbol{A}}_E[\mathrm{diag}(\boldsymbol{I} - \hat{\boldsymbol{C}}\boldsymbol{m})]^{-1}\boldsymbol{m} = \hat{\boldsymbol{A}}_E\hat{\boldsymbol{B}}(\boldsymbol{m})\boldsymbol{m}, \\ \boldsymbol{h}^a_{\mathrm{QA}} &= \hat{\boldsymbol{A}}_H[\mathrm{diag}(\boldsymbol{I} - \hat{\boldsymbol{C}}\boldsymbol{m})]^{-1}\boldsymbol{m} = \hat{\boldsymbol{A}}_H\hat{\boldsymbol{B}}(\boldsymbol{m})\boldsymbol{m}, \end{aligned} \tag{63}$$

where

$$\hat{\boldsymbol{A}}_E = \hat{\boldsymbol{G}}_E\hat{e}^b, \qquad \hat{\boldsymbol{A}}_H = \hat{\boldsymbol{G}}_H\hat{e}^b, \tag{64}$$

and diagonal matrix

$$\hat{\boldsymbol{B}}(\boldsymbol{m}) = [\mathrm{diag}(\boldsymbol{I} - \hat{\boldsymbol{C}}\boldsymbol{m})]^{-1}. \tag{65}$$

Let us introduce a notation $\boldsymbol{d}$ for an electric or magnetic vector of the anomalous part of the observed data. This vector contains the components of the anomalous electric and/or magnetic fields at the receivers. Using these notations, the forward modelling problem for the EM field can be expressed by the following matrix operation:

$$\boldsymbol{d} = \hat{\boldsymbol{A}}[\mathrm{diag}(\boldsymbol{I} - \hat{\boldsymbol{C}}\boldsymbol{m})]^{-1}\boldsymbol{m} = \hat{\boldsymbol{A}}\hat{\boldsymbol{B}}(\boldsymbol{m})\boldsymbol{m}, \tag{66}$$

where $\hat{\boldsymbol{A}}$ stands for the electric or magnetic matrices, $\hat{\boldsymbol{A}}_E = \hat{\boldsymbol{G}}_E\hat{e}^b$ or $\hat{\boldsymbol{A}}_H = \hat{\boldsymbol{G}}_H\hat{e}^b$, respectively.

Now let us consider the derivation of the Frechet derivative matrix of the forward operator (66). Taking into account that the model parameters are the anomalous conductivity values in the cells of the anomalous body, matrix $\hat{\boldsymbol{A}}$ is independent of the model parameters and $\hat{\boldsymbol{B}}$ is a diagonal matrix, one can express the perturbation of the forward operator (66) with respect to the model parameters in the form

$$\delta\boldsymbol{d} = \hat{\boldsymbol{A}}\delta[\hat{\boldsymbol{B}}(\boldsymbol{m})\boldsymbol{m}] = \hat{\boldsymbol{A}}\{\hat{\boldsymbol{B}}(\boldsymbol{m})\delta\boldsymbol{m} + \mathrm{diag}(\boldsymbol{m})\delta[\hat{\boldsymbol{B}}(\boldsymbol{m})]\}.$$

Since

$$\begin{aligned} \delta[\hat{\boldsymbol{B}}(\boldsymbol{m})] &= \delta[\mathrm{diag}(\boldsymbol{I} - \hat{\boldsymbol{C}}\boldsymbol{m})]^{-1} \\ &= [\mathrm{diag}(\boldsymbol{I} - \hat{\boldsymbol{C}}\boldsymbol{m})]^{-2}\hat{\boldsymbol{C}}\delta\boldsymbol{m} \\ &= \hat{\boldsymbol{B}}^2(\boldsymbol{m})\hat{\boldsymbol{C}}\delta\boldsymbol{m}, \end{aligned}$$

we obtain

$$\delta d = \hat{A}\{\hat{B}(m) + \mathrm{diag}(m)\hat{B}^2(m)\hat{C}\}\delta m = \hat{F}(m)\delta m,$$

where

$$\hat{F}(m) = \hat{A}\ \{\hat{B}(m) + \mathrm{diag}(m)\hat{B}^2(m)\hat{C}\} \tag{67}$$

is the Frechet derivative matrix.

Note that the terms depending on the model parameters are diagonal matrices. The full matrices $\hat{A}$ and $\hat{C}$ depend only on the background conductivity distribution. Therefore, after precomputing full matrices $\hat{A}$ and $\hat{C}$ for the background model, the iterative updating of $F(m)$ is relatively inexpensive during the inversion process.

## Appendix B. RCG method for the solution of the nonlinear inverse problem

The discrete nonlinear inverse problem can be formulated as follows:

$$d = G(m),$$

where $G$ is, in general, a nonlinear forward operator, $m$ is a vector of model parameters and $d$ is a vector of the observed data.

For regularized solution of a nonlinear inverse problem, we introduce a parametric functional

$$\begin{aligned} P^{\alpha}(m) &= \|\hat{W}_d A(m) - \hat{W}_d d\|^2 + \alpha\|\hat{W}_m m - \hat{W}_m m_{\mathrm{apr}}\|^2 \\ &= (\hat{W}_d A(m) - \hat{W}_d d)^*(\hat{W}_d A(m) - \hat{W}_d d) \\ &\quad +\alpha(\hat{W}_m m - \hat{W}_m m_{\mathrm{apr}})^*(\hat{W}_m m - \hat{W}_m m_{\mathrm{apr}}), \end{aligned}$$

where $\hat{W}_d$ and $\hat{W}_m$ are some weighting matrices of data and model parameters; $m_{\mathrm{apr}}$ is some *a priori* model.

According to the basic principles of the regularization method (Tikhonov and Arsenin 1977, Zhdanov 1993), we have to find the model $m_{\alpha}$, a quasi-solution of the inverse problem, that minimizes the parametric functional

$$P^{\alpha}(m) = \min .$$

The RCG method is described by the following iteration process (Zhdanov 1993):

$$m_{n+1} = m_n + \delta m = m_n - k_n^{\alpha}\tilde{l}^{\alpha}(m_n), \tag{68}$$

where the 'directions' of ascent $\tilde{l}^{\alpha}(m_n)$ are selected according to the algorithm described below.

In the initial step, we use the 'direction' of regularized steepest ascent for initial model $m_0$:

$$\tilde{l}^{\alpha}(m_0) = l^{\alpha}(m_0) = \hat{F}_{m_0}^{*}\hat{W}_d^2(A(m_0) - d) + \alpha\hat{W}_m^2(m_0 - m_{\mathrm{apr}}),$$

where $\hat{F}_{m_0}$ is the Frechet derivative matrix for the initial model.

In the next step, the 'direction' of ascent is the linear combination of the regularized steepest ascent on this step and the 'direction' of ascent $\tilde{l}^{\alpha}(m_0)$ on the previous step:

$$\tilde{l}^{\alpha}(m_1) = l^{\alpha}(m_1) + \beta_1^{\alpha}\tilde{l}^{\alpha}(m_0).$$

In the $(n+1)$th step

$$\tilde{l}^{\alpha}(m_{n+1}) = l^{\alpha}(m_{n+1}) + \beta_{n+1}^{\alpha}\tilde{l}^{\alpha}(m_n), \tag{69}$$

where the regularized steepest ascent directions are determined now according to the formula

$$l^{\alpha}(m_n) = \hat{F}^{*}_{m_n}\hat{W}_d^2(G(m_n) - d) + \alpha\hat{W}^2_{m_n}(m_n - m_{\mathrm{apr}}) \tag{70}$$

and $\hat{F}_{m_n}$ is the Frechet derivative matrix computed on the $n$th iteration.

The length of iteration step, a coefficient $k_n^{\alpha}$, can be determined based on the linear or parabolic line search:

$$P^{\alpha}(m_{n+1}) = P^{\alpha}(m_n - k_n^{\alpha}\tilde{l}^{\alpha}(m_n)) = f(k_n^{\alpha}) = \min .$$

The solution of this minimization problem gives the following best estimation for the length of the step using a linear line search:

$$k_n^{\alpha} = \frac{\tilde{l}^{\alpha *}(m_n) l^{\alpha}(m_n)}{\tilde{l}^{\alpha *}(m_n)(\hat{F}^{*}_{m_n}\hat{W}_d^2\hat{F}_{m_n} + \alpha\hat{W}_m^2)\tilde{l}^{\alpha}(m_n)}. \tag{71}$$

One can use a parabolic line search also (Fletcher 1981) to improve the convergence rate of the RCG method.

The CG method requires that the vectors $\tilde{l}^{\alpha}(m_n)$ introduced above will be mutually conjugate. This requirement is fulfilled if the coefficients $\beta_n$ are determined by the formula (Tarantola 1987)

$$\beta_{n+1}^{\alpha} = \frac{\|l^{\alpha}(m_{n+1})\|^2}{\|l^{\alpha}(m_n)\|^2}.$$

Using equations (68), (70) and (71), we can obtain $m$ iteratively.

The regularization parameter $\alpha$ describes the trade-off between the best fitting and most reasonable stabilization. In a case when $\alpha$ is selected to be too small, the minimization of the parametric functional $P^{\alpha}(m)$ is equivalent to the minimization of the misfit functional $\phi(m)$; therefore we have no regularization, which can result in an unstable incorrect solution. When $\alpha$ is too large, the minimization of the parametric functional $P^{\alpha}(m)$ is equivalent to the minimization of the stabilizing functional $S(m)$, which will force the solution to be closer to the *a priori* model. Ultimately, we would expect the final model to be exactly like the *a priori* model, while the observed data are totally ignored in the inversion. Thus, the critical question in the regularized solution of the inverse problem is the selection of the optimal regularization parameter $\alpha$. The basic principles used for determining the regularization parameter $\alpha$ are discussed in Tikhonov and Arsenin (1977) and Zhdanov (1993).

We use a simple numerical method to determine the parameter $\alpha$. Consider, for example, the progression of numbers

$$\alpha_k = \alpha_0 q^k; \qquad k = 0, 1, 2, \ldots, n; \qquad q > 0. \tag{72}$$

For any number $\alpha_k$ we can find an element $m_{\alpha_k}$, minimizing $P^{\alpha_k}(m)$, and calculate the misfit $\|G(m_{\alpha_k}) - d\|^2$. The optimal value of the parameter $\alpha$ is the number $\alpha_{k0}$, for which we have

$$\|G(m_{\alpha_{k0}}) - d\|^2 = \delta, \tag{73}$$

where $\delta$ is the level of noise in the observed data. The equality (73) is called *the misfit condition*.

In our code we use the following algorithm of the RCG method:

$$\tilde{l}^{\alpha_{n+1}}(m_{n+1}) = l^{\alpha_{n+1}}(m_{n+1}) + \beta_{n+1}\tilde{l}^{\alpha_n}(m_n),$$

where $\alpha_n$ are the subsequent values of the regularization parameter. This method is called the *adaptive* regularization method (Tikhonov and Arsenin 1977). In order to avoid divergence, we begin an iteration from a value of $\alpha_0$, which can be obtained as a ratio of the misfit functional and stabilizer for an initial model, then reduce $\alpha_n$ according to formula (72) on each subsequent iteration and continuously iterate until the misfit condition (73) is reached.

## Appendix C. Re-weighted RCG method in the space of weighted parameters

The re-weighted RCG method is based on a successive line search of the minimum of the parametric functional (52) in the RCG direction $\vec{\tilde{l}}^{\alpha}_{w}(\boldsymbol{m}^{w}_{n})$:

$$\boldsymbol{m}^{w}_{n+1} = \boldsymbol{m}^{w}_{n} + \delta\boldsymbol{m}^{w} = \boldsymbol{m}^{w}_{n} - k^{\alpha}_{n}\vec{\tilde{l}}^{\alpha}_{w}(\boldsymbol{m}^{w}_{n}).$$

The iteration step (coefficient $k^{\alpha}_{n}$) is determined from the linear line search:

$$k_n = \frac{\tilde{\boldsymbol{l}}^{\alpha *}_{w}(\boldsymbol{m}^{w}_{n})\boldsymbol{l}^{\alpha}_{w}(\boldsymbol{m}^{w}_{n})}{\tilde{\boldsymbol{l}}^{\alpha *}_{w}(\boldsymbol{m}^{w}_{n})(\hat{\boldsymbol{F}}^{*}_{wn}\hat{\boldsymbol{W}}^{2}_{d}\hat{\boldsymbol{F}}_{wn} + \alpha\hat{\boldsymbol{I}})\tilde{\boldsymbol{l}}^{\alpha}_{w}(\boldsymbol{m}^{w}_{n})}, \tag{74}$$

where $\hat{\boldsymbol{F}}^{*}_{wn}$ is the Frechet derivative matrix of the operator $\hat{\boldsymbol{W}}_d\boldsymbol{G}(\hat{\boldsymbol{W}}^{-1}_{m}\hat{\boldsymbol{W}}_{en}\boldsymbol{m}^{w})$. We can also use a parabolic line search for $k^{\alpha}_{n}$ (Fletcher 1981).

According to (51), it is equal to

$$\hat{\boldsymbol{F}}_{wn} = \hat{\boldsymbol{W}}_d\hat{\boldsymbol{F}}_n\hat{\boldsymbol{W}}^{-1}_{m}\hat{\boldsymbol{W}}_{en}. \tag{75}$$

The RCG directions $\vec{\tilde{l}}^{\alpha}_{w}(\boldsymbol{m}^{w}_{n})$ are selected according to the same rules as for the conventional RCG method presented in appendix B.

In the first step we use the steepest ascent direction:

$$\vec{\tilde{l}}^{\alpha}_{w}(\boldsymbol{m}^{w}_{0}) = \boldsymbol{l}^{\alpha}_{w}(\boldsymbol{m}^{w}_{0}) = \hat{\boldsymbol{W}}_{e0}\hat{\boldsymbol{W}}^{-1}_{m}\hat{\boldsymbol{F}}^{*}_{0}\hat{\boldsymbol{W}}_d(\boldsymbol{G}^{w}(\boldsymbol{m}^{w}_{0}) - \boldsymbol{d}^{w}) + \alpha(\boldsymbol{m}^{w}_{0} - \boldsymbol{m}^{w}_{\mathrm{apr}}), \tag{76}$$

where $\boldsymbol{F}_{m_0}$ is the Frechet derivative matrix for the initial model.

In the $(n+1)$th step, the 'direction' of ascent, $\tilde{\boldsymbol{l}}^{\alpha}_{w}(\boldsymbol{m}^{w}_{n+1})$, is the linear combination of the regularized steepest ascent, $\boldsymbol{l}^{\alpha}_{w}(\boldsymbol{m}^{w}_{n+1})$, in this step and the 'direction' of ascent, $\tilde{\boldsymbol{l}}^{\alpha}_{w}(\boldsymbol{m}^{w}_{n})$, in the previous step:

$$\tilde{\boldsymbol{l}}^{\alpha}_{w}(\boldsymbol{m}^{w}_{n+1}) = \boldsymbol{l}^{\alpha}_{w}(\boldsymbol{m}^{w}_{n+1}) + \beta^{\alpha}_{n+1}\tilde{\boldsymbol{l}}^{\alpha}_{w}(\boldsymbol{m}^{w}_{n}). \tag{77}$$

The regularized steepest ascent directions for the re-weighted RCG method are determined according to the formula

$$\boldsymbol{l}^{\alpha}_{w}(\boldsymbol{m}^{w}_{n}) = \hat{\boldsymbol{W}}_{en}\hat{\boldsymbol{W}}^{-1}_{m}\hat{\boldsymbol{F}}^{*}_{n}\hat{\boldsymbol{W}}_d(\boldsymbol{G}^{w}(\boldsymbol{m}^{w}_{n}) - \boldsymbol{d}^{w}) + \alpha(\boldsymbol{m}^{w}_{n} - \boldsymbol{m}^{w}_{\mathrm{apr}}),$$

where

$$\hat{\boldsymbol{W}}_{en} = \mathrm{diag}[(\boldsymbol{m}_n - \boldsymbol{m}_{\mathrm{apr}})^2 + \varepsilon^2\boldsymbol{I}]^{1/2} \approx \mathrm{diag}(|\boldsymbol{m}_n - \boldsymbol{m}_{\mathrm{apr}}|). \tag{78}$$

The coefficients $\beta^{\alpha}_{n+1}$ are defined from the condition that the directions $\tilde{\boldsymbol{l}}^{\alpha}_{w}(\boldsymbol{m}^{w}_{n+1})$ and $\tilde{\boldsymbol{l}}^{\alpha}_{w}(\boldsymbol{m}^{w}_{n})$ are conjugate (Tarantola 1987):

$$\beta_{n+1} = \frac{\|\boldsymbol{l}^{\alpha}_{w}(\boldsymbol{m}_n)\|^2}{\|\boldsymbol{l}^{\alpha}_{w}(\boldsymbol{m}_{n-1})\|^2}. \tag{79}$$

Note that at each step we re-compute the real parameters of the model from the weighted parameters at the $n$th iteration:

$$\boldsymbol{m}_{n+1} = \hat{\boldsymbol{W}}^{-1}_{m}\hat{\boldsymbol{W}}_{en}\boldsymbol{m}^{w}_{n+1}. \tag{80}$$

We call this algorithm the re-weighted RCG method because the weighting matrix $\hat{\boldsymbol{W}}_{en}$ is updated on each iteration. One can find the formal proof of the convergence of this type of optimization technique in Eckhart (1980).

The iterative process is terminated when the misfit reaches the given level $\varepsilon_0$:

$$\phi(\boldsymbol{m}_N) = \|\boldsymbol{r}_N\|^2 \leqslant \varepsilon_0.$$

Note that, in the practical implementation of the re-weighted RCG method, we update the weights, matrix $\hat{\boldsymbol{W}}^{-1}_{en}$ and the regularization parameter, $\alpha_n$, not on every iteration, but after performing a sequence of iterations (usually five or ten) with the fixed values of $\hat{W}_{en_0}^{-1}$ and $\alpha_{n_0}$. This improves the convergence rate and robustness of the algorithm, keeping the value of the regularization parameter $\alpha_n$ from being too small during the iteration process.

Numerical tests show that the MS functional generates a stable solution but it tends to produce the smallest possible anomalous domain. Following Portniaguine and Zhdanov (1999), we now impose the upper boundary $\Delta\sigma^+(\boldsymbol{r})$ and the lower boundary $\Delta\sigma^-(\boldsymbol{r})$ for the conductivity values $\Delta\sigma(\boldsymbol{r})$ determined as a result of inversion. During the iterative process we simply cut off all the values outside these boundaries. This algorithm can be described by the following formula:

$$\begin{aligned} \Delta\sigma(\boldsymbol{r}) &= \Delta\sigma^+(\boldsymbol{r}), \qquad \text{if} \quad \Delta\sigma(\boldsymbol{r}) \geqslant \Delta\sigma^+(\boldsymbol{r}) \\ \Delta\sigma(\boldsymbol{r}) &= \Delta\sigma^-(\boldsymbol{r}), \qquad \text{if} \quad \Delta\sigma(\boldsymbol{r}) \leqslant \Delta\sigma^-(\boldsymbol{r}). \end{aligned} \tag{81}$$

Thus, according to the last formula the anomalous conductivities $\Delta\sigma(\boldsymbol{r})$ are always distributed within the interval

$$\Delta\sigma^-(\boldsymbol{r}) \leqslant \Delta\sigma(\boldsymbol{r}) \leqslant \Delta\sigma^+(\boldsymbol{r}).$$

## References


Alumbaugh D L and Newman G A 1997 Three-dimensional massively parallel inversion II. Analysis of a cross-well electromagnetic experiment *Geophys. J. Int.* **128** 355–63

Avdeev D, Kuvshinov A, Pankratov O and Newman G A 1998 Three-dimensional frequency domain modelling of airborne electromagnetic responses *Exploration Geophys.* **29** 111–19

Berdichevsky M N and Zhdanov M S 1984 *Advanced Theory of Deep Geomagnetic Sounding* (Amsterdam: Elsevier)

Born M 1933 *Optics* (Berlin: Springer)

Constable S C, Parker R C and Constable G G 1987 Occam's inversion: a practical algorithm for generating smooth models from EM sounding data *Geophysics* **52** 289–300

Dmitriev V I and Pozdnyakova E E 1992 Method and algorithm for computing the EM field in a stratified medium with a local inhomogeneity in an arbitrary layer *Comput. Math.* **3** 181–8

Druskin V, Knizhnerman L and Lee P 1999 New spectral Lanczos decomposition method for induction modelling in arbitrary 3D geometry *Geophysics* **64** 701–6

Eaton P A 1989 3D EM inversion using integral equations *Geophys. Prosp.* **37** 407–26

Eckhart U 1980 Weber's problem and Weiszfeld's algorithm in general spaces *Math. Programming* **18** 186–208

Fletcher R 1981 *Practical Methods of Optimization* (New York: Wiley)

Golubev N, Zhdanov M S, Matsuo K and Negi T 1999 Three-dimensional inversion of magnetotelluric data over Minami-Noshiro oil field *Proc. 2nd Int. Symp. of Three-Dimensional Electromagnetics 1999 (Salt Lake City, UT)* pp 305–8

Habashy T M, Chew W C and Chow E Y 1986 Simultaneous reconstruction of permittivity and conductivity profiles in a radially inhomogeneous slab *Radio Sci.* **21** 635–45

Habashy T M, Groom R W and Spies B R 1993 Beyond the Born and Rytov approximations: a nonlinear approach to electromagnetic scattering *J. Geophys. Res.* **98** 1759–75

Hohmann G W 1975 3D induced polarization and EM modelling *Geophysics* **40** 309–24

Lee K H and Xie G 1993 A new approach to imaging with low frequency EM fields *Geophysics* **58** 780–96

Madden T R and Mackie R L 1989 3D magnetotelluric modelling and inversion *Proc. IEEE* **77** 318–32

Mehanee S, Golubev N and Zhdanov M S 1998 Weighted regularized inversion of magnetotelluric data *Expanded Abstracts SEG 68th Annual Meeting (New Orleans)* pp 481–4

Nekut A 1994 EM ray-trace tomography *Geophysics* **59** 371–7

Newman G A and Alumbaugh D L 1997 Three-dimensional massively parallel inversion: I. Theory *Geophys. J. Int.* **128** 355–63

Oristaglio M, Wang T, Hohmann G W and Tripp A 1993 Resistivity imaging of transient EM data by conjugate-gradient method *SEG Abstracts* (Washington DC: SEG) pp 347–50

Oristaglio M L 1989 An inverse scattering formula that uses all the data *Inverse Problems* **5** 1097–105

Pellerin L, Johnston J and Hohmann G W 1993 3D inversion of EM data *SEG Abstracts* (Washington, DC: SEG) pp 360–63

Portniaguine O and Zhdanov M S 1999 Focusing geophysical inversion images *Geophysics* **64** 874–87

Rudin L I, Osher S and Fatemi E 1992 Nonlinear total variation based noise removal algorithms *Physica* D **60** 259–68

Smith J T and Booker J R 1991 Rapid inversion of 2 and 3D magnetotelluric data *J. Geophys. Res.* **96** 3905–22

Tarantola A 1987 *Inverse Problem Theory* (Amsterdam: Elsevier)

Tikhonov A N and Arsenin V Y 1977 *Solution of Ill-Posed Problems* (New York: Winston and Sons)

Torres-Verdin C and Habashy T M 1994 Rapid 2.5-dimensional forward modelling and inversion via a new nonlinear scattering approximation *Radio Sci.* **29** 1051–79

Vogel C R and Oman M E 1998 A fast, robust total-variation based reconstruction of noisy, blurred images *IEEE Trans. Image Processing* **7** 813–24

Wannamaker P E 1991 Advances in 3D magnetotelluric modelling using integral equations *Geophysics* **56** 1716–28

Weidelt P 1975 EM induction in 3D structures *J. Geophys.* **41** 85–109

Xie G and Lee K H 1995 Nonlinear inversion of 3D EM data *PIERS Proc. The University of Washington* p 323

Xiong Z 1992 EM modelling of 3D structures by the method of system iteration using integral equations *Geophysics* **57** 1556–61

Zhdanov M S 1993 *Tutorial: Regularization in Inversion Theory* (Colorado School of Mines) p 47

Zhdanov M S, Dmitriev V I, Fang S and Hursan G 1999 Quasi-analytical approximations and series in electromagnetic modelling *Geophysics* at press

Zhdanov M S and Fang S 1996a Quasi-linear approximation in 3D EM modelling *Geophysics* **61** 646–65

——1996b 3D quasi-linear EM inversion *Radio Sci.* **31** 741–54

——1997 Quasi linear series in 3D EM modelling *Radio Sci.* **32** 2167–88

——1999 3D quasi-linear electromagnetic modelling and inversion *Three Dimensional Electromagnetics (SEG Monograph)* (Tulsa, OK: SEG) pp 233–55

Zhdanov M S and Keller G 1994 *The Geoelectrical Methods in Geophysical Exploration* (Amsterdam: Elsevier) p 873